

**Supplementary Materials for**  
**The synergic effects at molecular level in CoS<sub>2</sub> for selective**  
**hydrogenation of nitroarenes**

Zhongzhe Wei,<sup>†</sup> Shanjun Mao,<sup>†</sup> Fanfei Sun,<sup>‡</sup> Jing Wang,<sup>†</sup> Bingbao Mei,<sup>‡</sup> Yiqing Chen,<sup>†</sup>  
Haoran Li,<sup>†</sup> Yong Wang<sup>\*,†</sup>

\*Corresponding author. Email: chemwy@zju.edu.cn

<sup>†</sup>Advanced Materials and Catalysis Group, ZJU-NHU United R&D Center, Department of Chemistry, Zhejiang University, Hangzhou 310028, P. R. China.

<sup>‡</sup>Shanghai Synchrotron Radiation Facility, Shanghai Institute of Applied Physics, Chinese Academy of Science, Shanghai 201204, P. R. China.

**This PDF file includes:**

Supplementary Figs 1-21  
Supplementary Tables 1-4

**Characterization.** TEM experiments were conducted on a Hitachi H7700 instrument, operating at 100 kV. HRTEM images were taken on Tecnai G2 F30 S-Twin, working on 300 kV. Scanning transmission electron microscopy (STEM) and high angle annular dark field (HAADF) imaging were utilized to observe the image of individual particle at atomic resolution with an aberration corrected JEOL 2200FS (S)TEM operating at 200 kV, in addition with the capability of taking X-ray energy dispersive spectrometer (EDS) spectra from individual particles larger than 1-2 nm. The BET surface area and pore volume were measured by N<sub>2</sub> adsorption-desorption experiments with a Micromeritics ASAP 2020 HD88. Powder XRD measurements were carried out on Model D/tex-Ultima TV using Cu Ka radiation (1.54 Å). The sample was scanned in the 2  $\theta$  range from 10° and 80°. The mean CoS<sub>2</sub> size in CoS<sub>2</sub>/PC was calculated from the Scherrer formula according to the 311 (2 $\theta$  = 54.3) diffraction lines in wide-angle XRD. XPS characterization was performed on an ESCALAB MARK II spherical analyzer with an aluminum anode (Al 1486.6 eV) X-ray source. ICP-AES measurements were conducted on PerkinElmer Optima OES 8000. EDS was applied to estimated the S content. XAFS measurements at Co k-edge in transmission mode were conducted at the BL14W1 in Shanghai Synchrotron Radiation Facility (SSRF). The electron beam energy was 3.5 GeV and the stored current was 230 mA (top-up). A 38-pole wiggler with the maximum magnetic field of 1.2 T inserted in the straight section of the storage ring was used. XAFS data were collected with a fixed-exit double-crystal Si(111) monochromator. The energy was calibrated by the Co foil. The photon flux at the sample position was 2.6×10<sup>12</sup> photons per second. The raw data analysis was proceeded with IFEFFIT software package according to the standard data analysis procedures. The spectra were calibrated, averaged, pre-edge background subtracted, and post-edge normalized using Athena program in IFEFFIT software package. The Fourier transformation of the  $k^3$ -weighted EXAFS oscillations,  $k^3 \cdot \chi(k)$ , from  $k$  space to R space was measured over a range of 3.5–11.5 Å<sup>-1</sup> to obtain a radial distribution function.

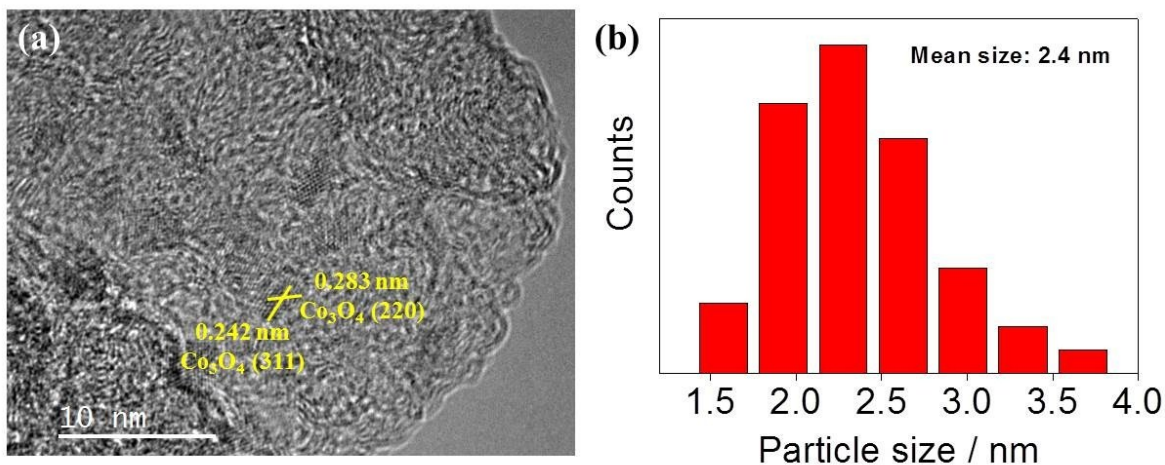


**Fig. S1.** HRTEM (a) and metal particle size distribution histogram (b) images of  $\text{Co}_3\text{O}_4/\text{PC}$ .

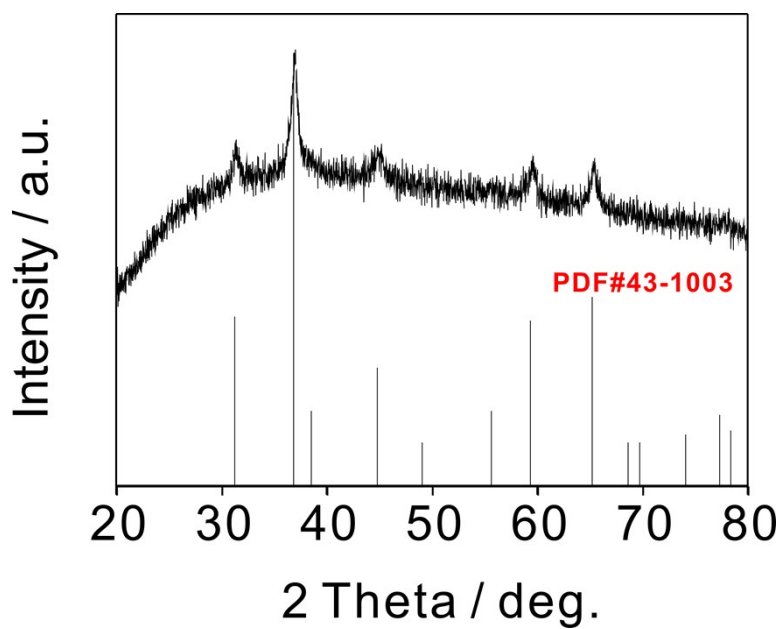


**Fig. S2.** XRD pattern of  $\text{Co}_3\text{O}_4/\text{PC}$ .

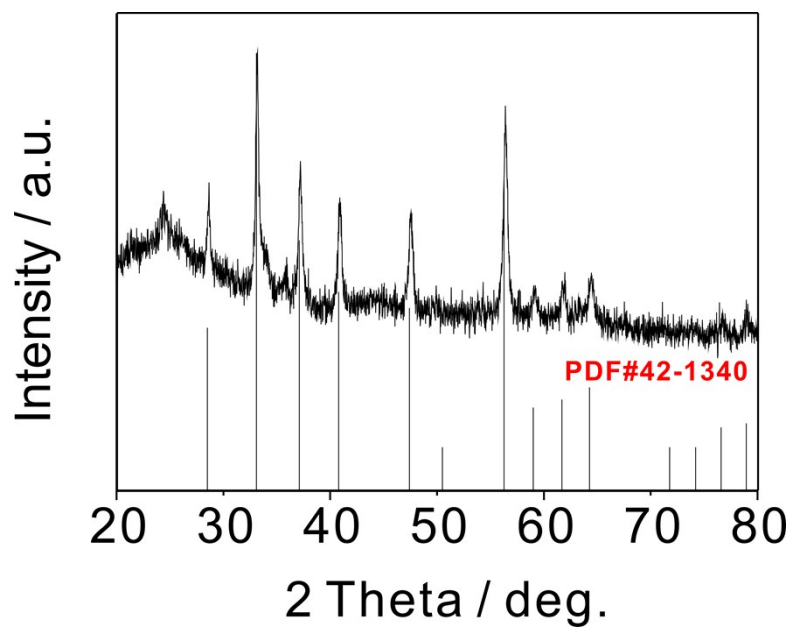


**Fig. S3.** XRD pattern of FeS<sub>2</sub>/PC.

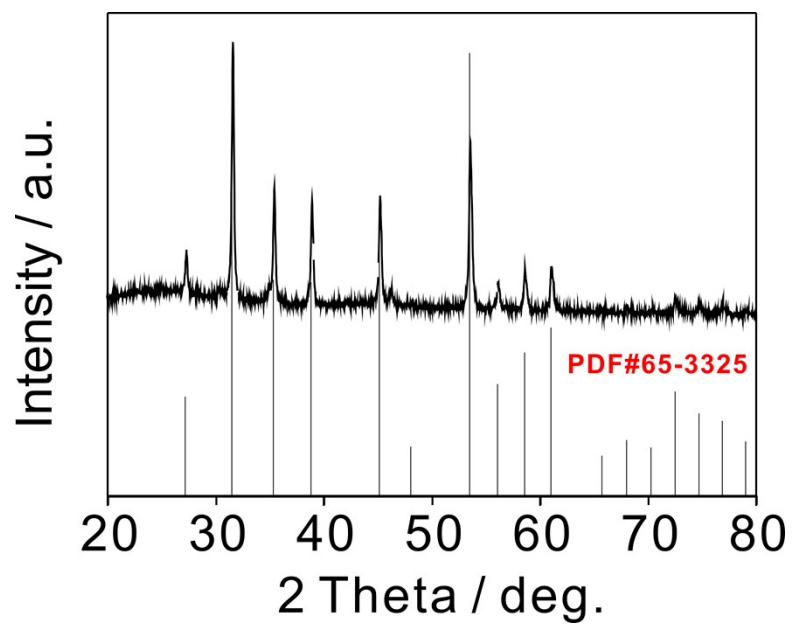


**Fig. S4.** XRD pattern of NiS<sub>2</sub>/PC.

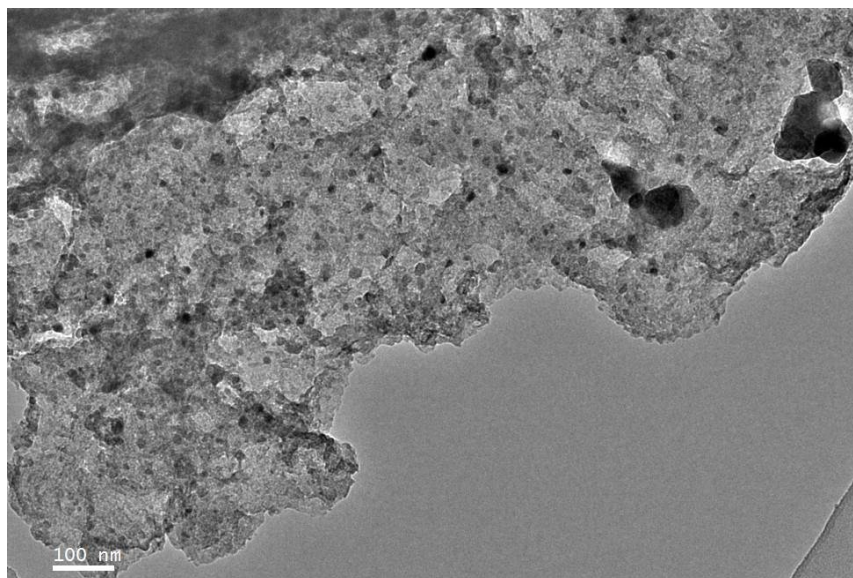


**Fig. S5.** TEM image of CoS<sub>2</sub>/PC.

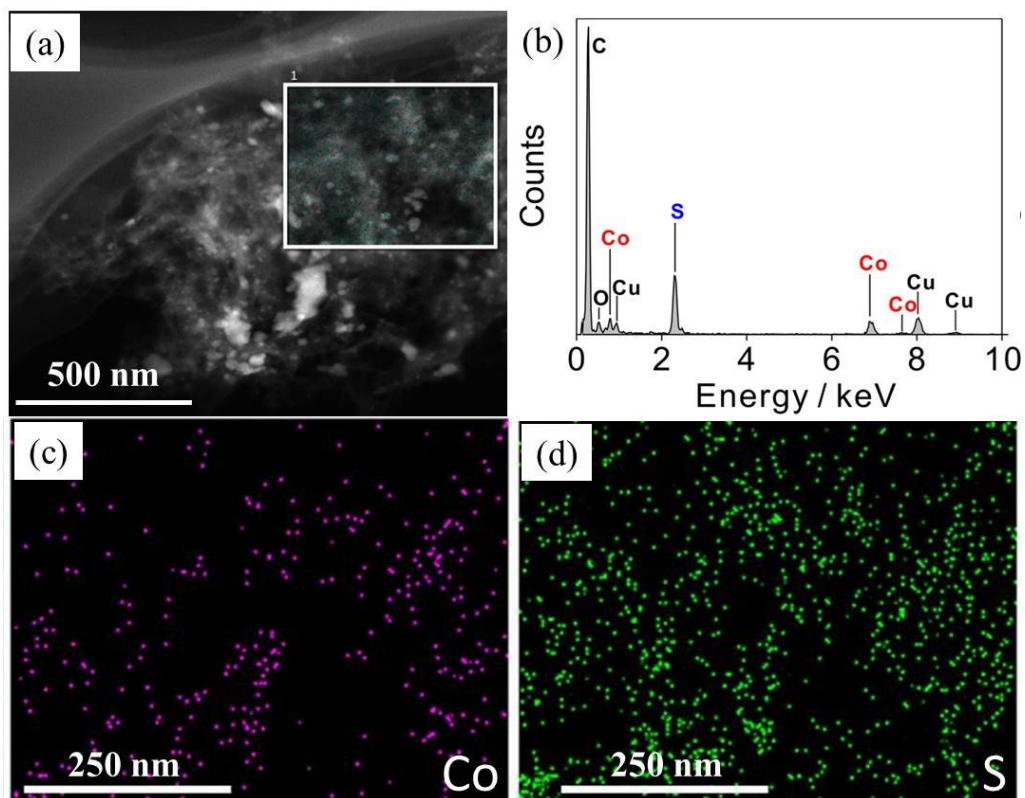


**Fig. S6.** A representative high-angle annular dark-field scanning transmission electron microscopy (HAADF-STEM) image (a) and the corresponding STEM-EDX point spectra (b) of CoS<sub>2</sub>/PC.

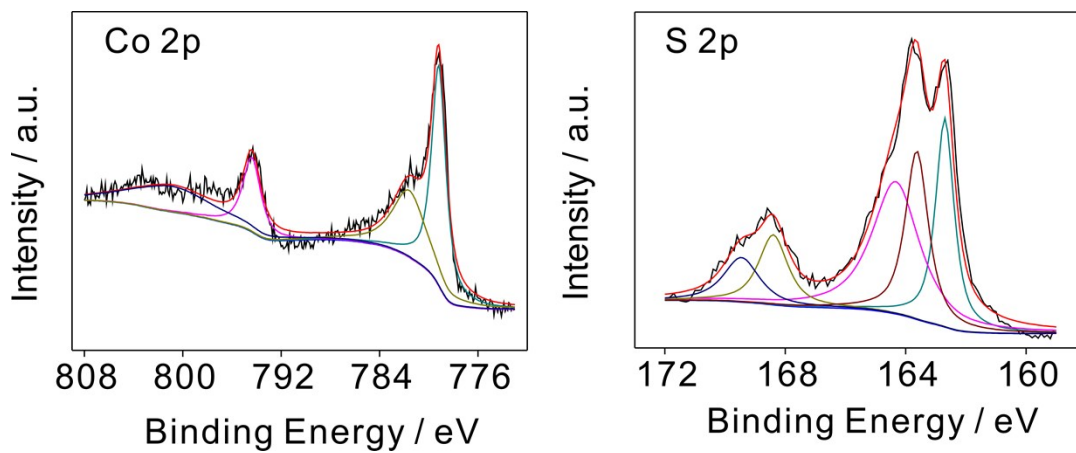


**Fig. S7.** XPS spectra of Co 2p core and S 2p core of CoS<sub>2</sub>/PC.

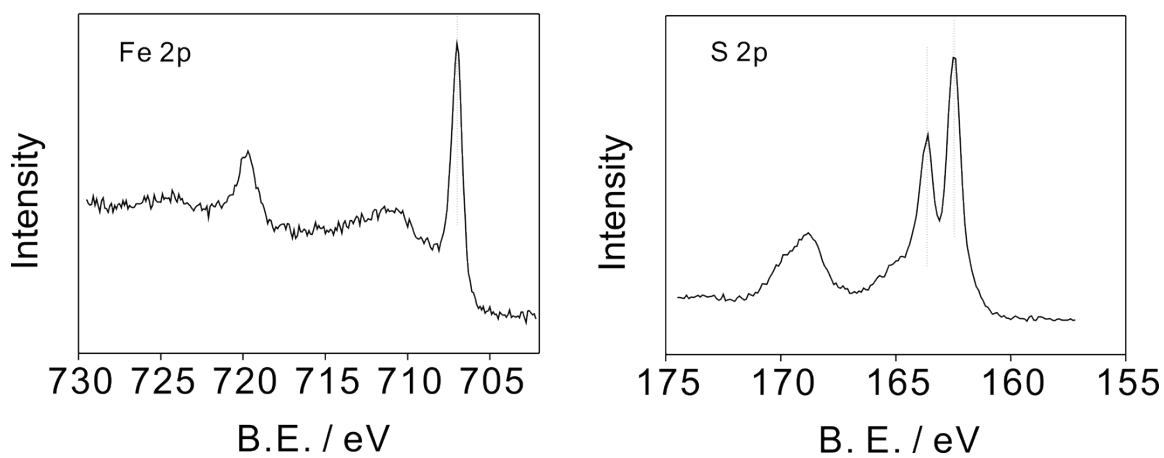


**Fig. S8.** XPS spectra of Fe 2p core and S 2p core of FeS<sub>2</sub>/PC.

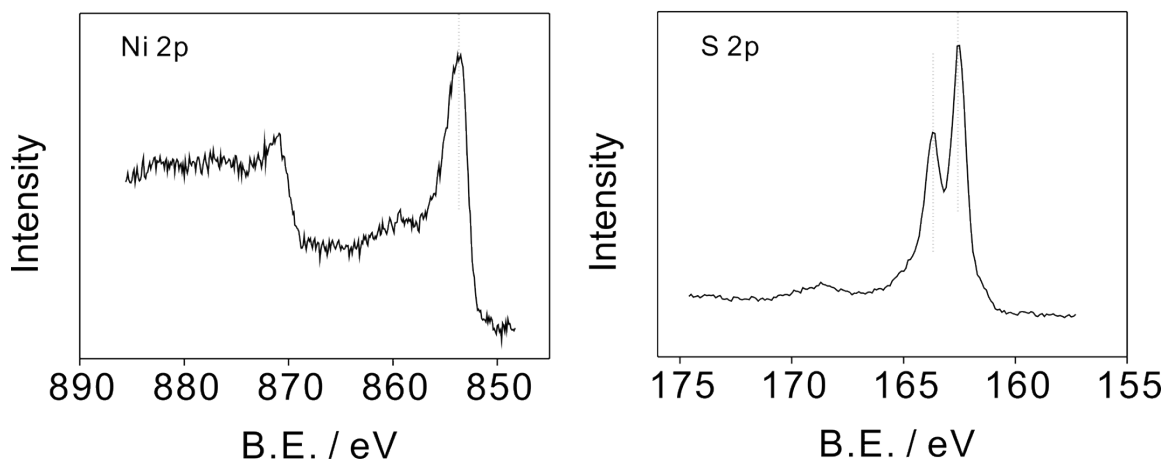


**Fig. S9.** XPS spectra of Ni 2p core and S 2p core of NiS<sub>2</sub>/PC.

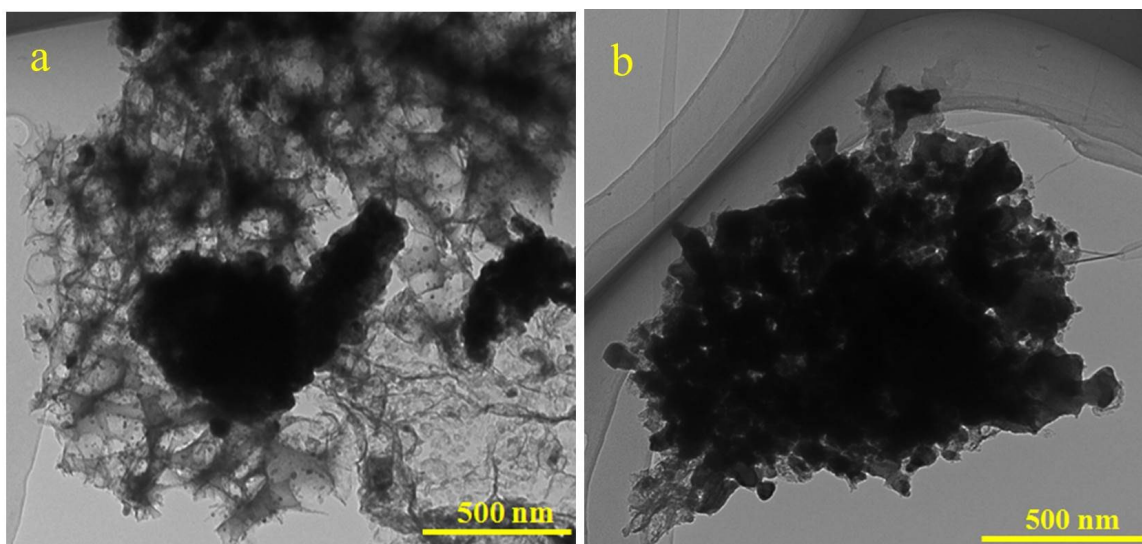


**Fig. S10.** TEM images of FeS<sub>2</sub>/PC (a) and NiS<sub>2</sub>/PC (b).

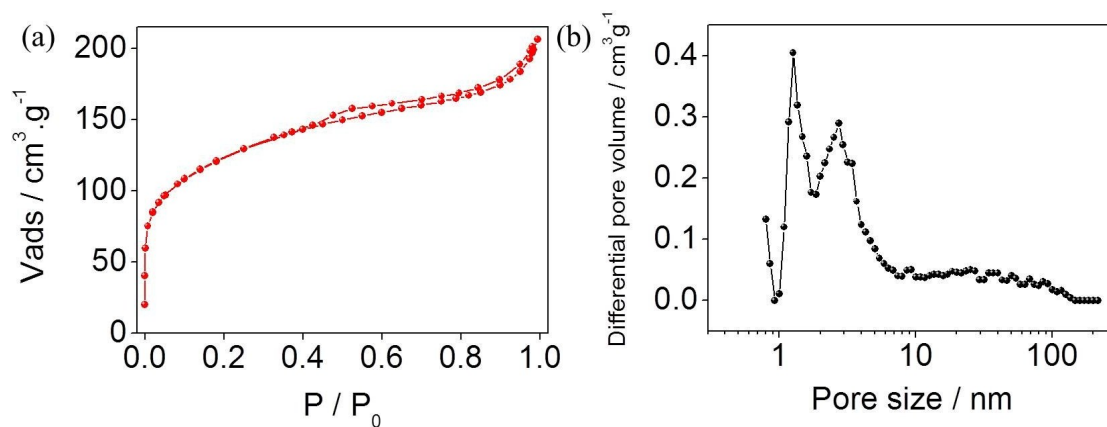


**Fig. S11.**  $N_2$  Adsorption/desorption isotherm (a) and the pore size distribution (b) of  $CoS_2/PC$ .

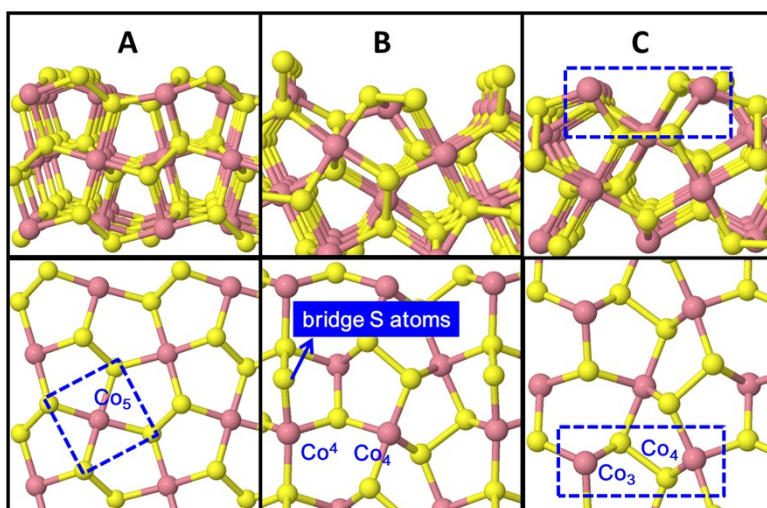


**Fig. S12.** The side and top view of the structures of two most stable surfaces for  $CoS_2$ . (A) (100), (B) (110) with bridged S atoms and (C) (110) without bridged S atoms.

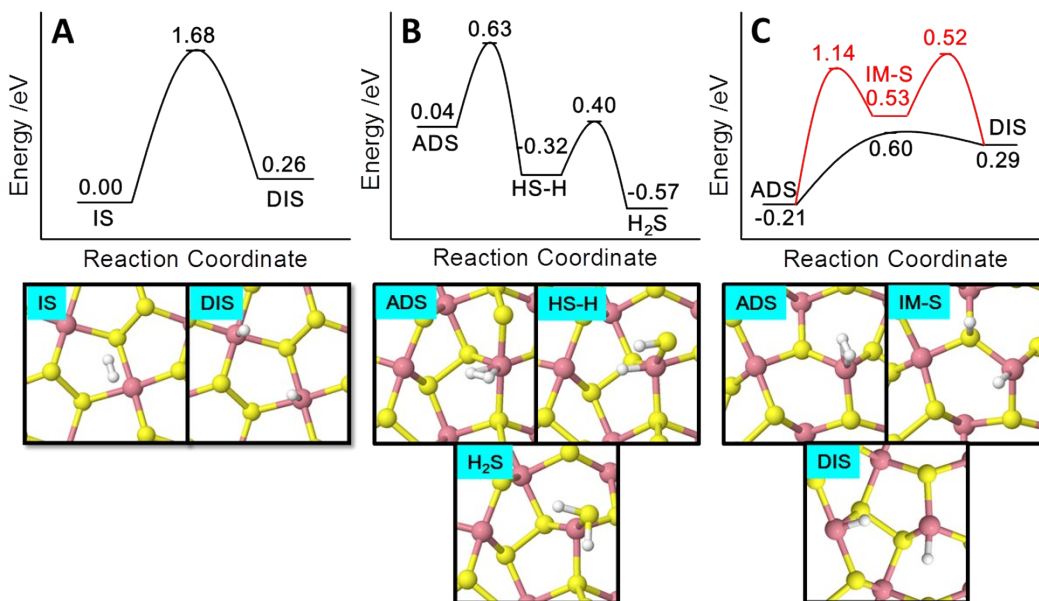


**Fig. S13.** (A)  $\text{H}_2$  activation at  $\text{Co}_5$  on (100); (B)  $\text{H}_2$  activation at  $\text{Co}^4$  on (110) and further interaction with bridge S atoms; (C)  $\text{H}_2$  activation at  $\text{Co}_3$  (black) and diffusion (red) on (110) without bridge S atoms.

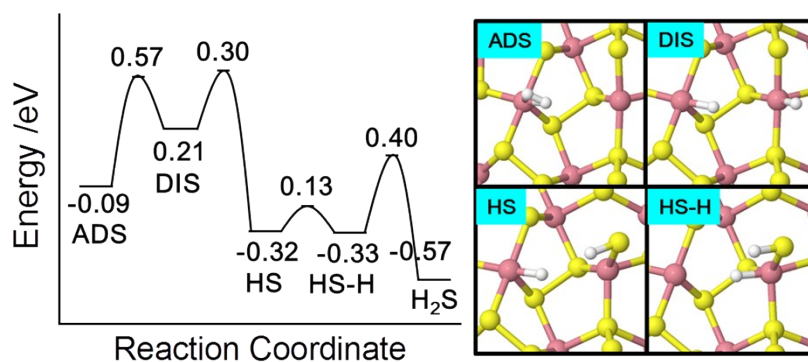


**Fig. S14.**  $\text{H}_2$  activation at  $\text{Co}_4$  on (110) and further interaction with bridge S atoms.

No stable molecular adsorption of  $\text{H}_2$  was found on (100), while the dissociated adsorption on  $\text{Co}_5$ 's is endothermic by 0.26 eV (Fig. S11A). Unfortunately, the dissociation barrier is as high as 1.68 eV, which makes it unlikely to be active surface compared with the energy profiles on (110) as we will discuss below. Molecular adsorption of  $\text{H}_2$  on  $\text{Co}^4$  and  $\text{Co}_4$  on (110) ends in a heat release of 0.04 and -0.09 eV (Figs. S11B and 12) respectively, indicating a weak binding. For  $\text{H}_2$  on  $\text{Co}^4$ , the

dissociation of H<sub>2</sub> will lead to the hydrogenation of bridge S with a barrier of 0.63 eV, forming adsorbed SH, then further addition of H to SH results in H<sub>2</sub>S (with a barrier of 0.40 eV), which implies that the bridge S will vanish at last, ending with the second (110) plane where Co<sub>3</sub> site occurs. Same results can be obtained for H<sub>2</sub> on Co<sub>4</sub> though more complex processes are involved (Fig. S12). Though the bridge S is reacted with H<sub>2</sub>, the catalyst didn't suffer from phase transformation as can be deduced from XRD (Fig. 1c). The resulted Co<sub>3</sub> site is much more active to H<sub>2</sub> molecular adsorption (with E<sub>ads</sub> of -0.21 eV, Fig. S11C).

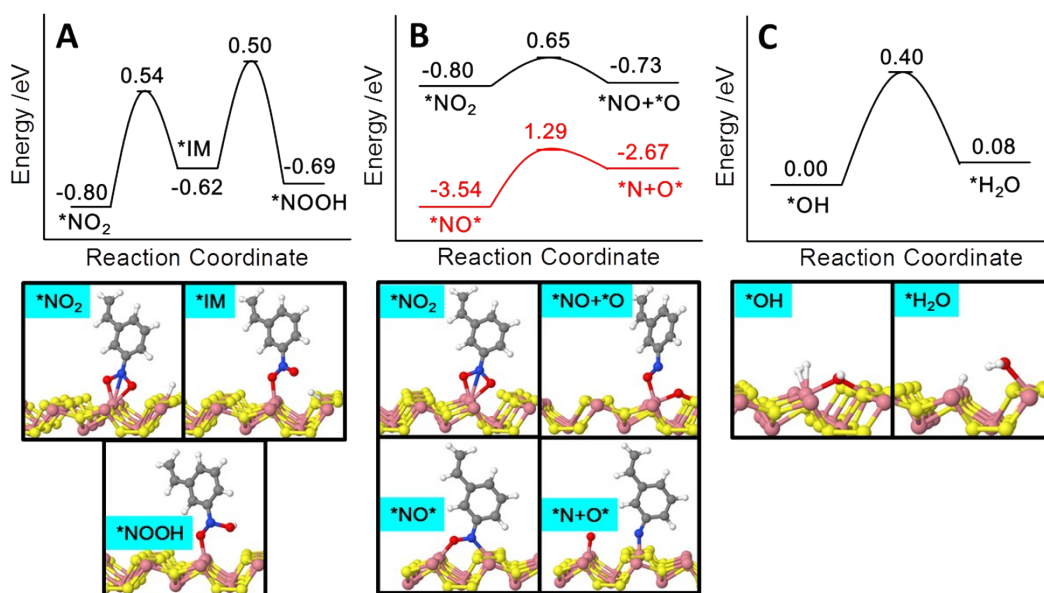


**Fig. S15.** (A) Activity of atomic H for the first hydrogenation step; (B) Deactivation mechanism of the catalyst with the low H<sub>2</sub> pressure; (C) The reduction of OH group left by NHOH.

Regarding the poisoning effect, the efficiency and deactivation of the CoS<sub>2</sub>/PC catalyst have to be stressed out. The biggest energy barrier along the most favorable reaction pathway is only 0.60 eV, quite comparable with that on the noble metal catalysts. However, much harsh conditions have to be applied to achieve considerable activity for CoS<sub>2</sub>/PC. The reason lies in the stronger adsorption of the substrate, intermediate, product compared to H<sub>2</sub>. Namely, H source supply is seriously suppressed by them. In

fact, the adsorption energy of NO rises to -1.85 eV if Co<sub>4</sub> site in the “synergic single-atom active site pair” is not occupied by H<sub>2</sub>. And the further conversion of NO becomes rather hard with a barrier up to 1.29 eV (Fig. S13B). Hence the activity or efficiency of CoS<sub>2</sub>/PC is greatly limited by the relative weak H<sub>2</sub> adsorption.

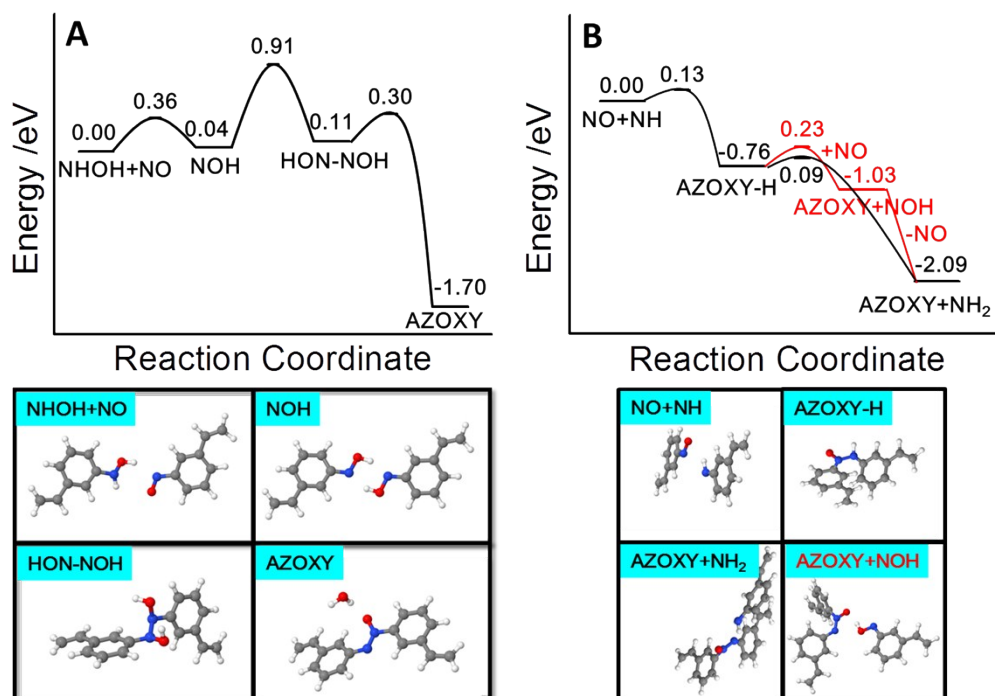


**Fig. S16.** Formation of AZOXY along the condensation route in absence of (A) and with (B) the catalyst.

DFT studies also reveal the participation of NO in solution along the possible condensation route with or in absence of the catalyst. Note that the  $E_{\text{ads}}$  of NHOH and the barrier for N and O bond breaking is similar. The formation of AZOXY may change accordingly with the presence of the catalyst since NO may react with NH as well. So the reaction pathways for the formation of AZOXY with and without the catalyst were studied from first principle. As seen in Fig. S14A, in absence of the catalyst, one H in NHOH was abstracted by NO, forming two NOH, then they bind together and release one molecular H<sub>2</sub>O to yield AZOXY. The decisive barrier for this pathway is as high as 0.91 eV. However, the bond between N and O will firstly break with catalyst (Fig. 4),

releasing NH into solution after overcoming a barrier of 0.31 eV. Then NH binds to NO, generating AZOXY-H (Fig. S14B). Lastly the H, binding with N in AZOXY, will be abstracted by another NH without any barrier, resulting in AZOXY and NH<sub>2</sub>. Or, considering the much amount of NO, H in AZOXY-H would be abstracted by NO with a barrier of only 0.23 eV, forming AZOXY and NOH. Then NOH would be re-oxidized to NO by NH, resulting in NH<sub>2</sub>. The biggest barrier (0.31 eV) along this way is much smaller than that without the catalyst, which helps explain the extreme efficiency for AZOXY generation in Fig. 6b. What's more, along the condensation route with CoS<sub>2</sub> catalyst, NO not only serves as the reactant, but also acts as the co-catalyst in the formation of AZOXY.

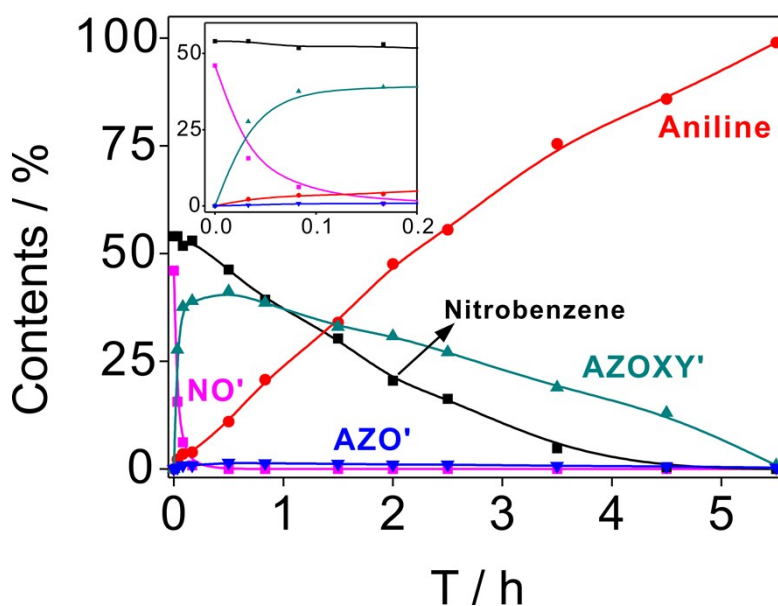


**Fig. S17.** Distribution of products during the hydrogenation of an equimolar mixture of nitrobenzene and nitrosobenzene. Reaction conditions: substrate (0.5 mmol), CoS<sub>2</sub>/PC (3.7 mol% Co), 3 MPa of H<sub>2</sub>, 110 °C.

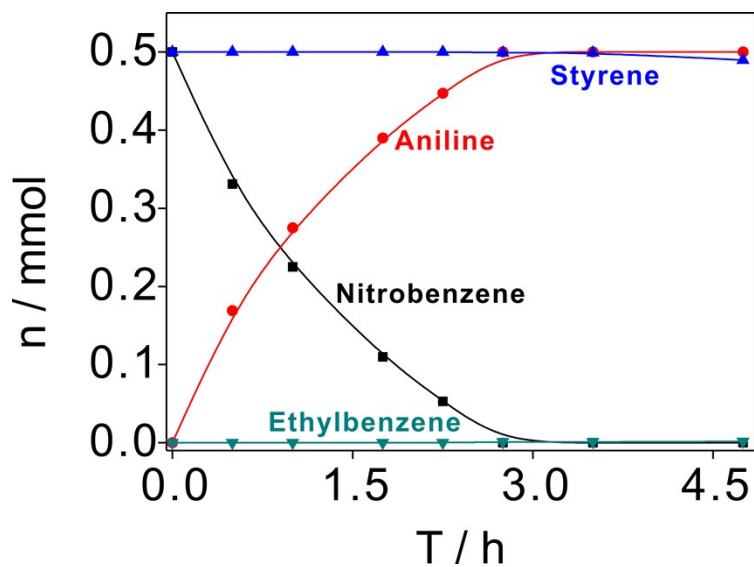


**Fig. S18.** Simultaneous hydrogenation of nitrobenzene and styrene on  $\text{CoS}_2/\text{PC}$ . Reaction conditions: nitrobenzene (0.5 mmol), styrene (0.5 mmol),  $\text{CoS}_2/\text{PC}$  (3.7 mol% Co),  $\text{CH}_3\text{OH}$  (5 mL), 3 MPa of  $\text{H}_2$ , 110 °C.

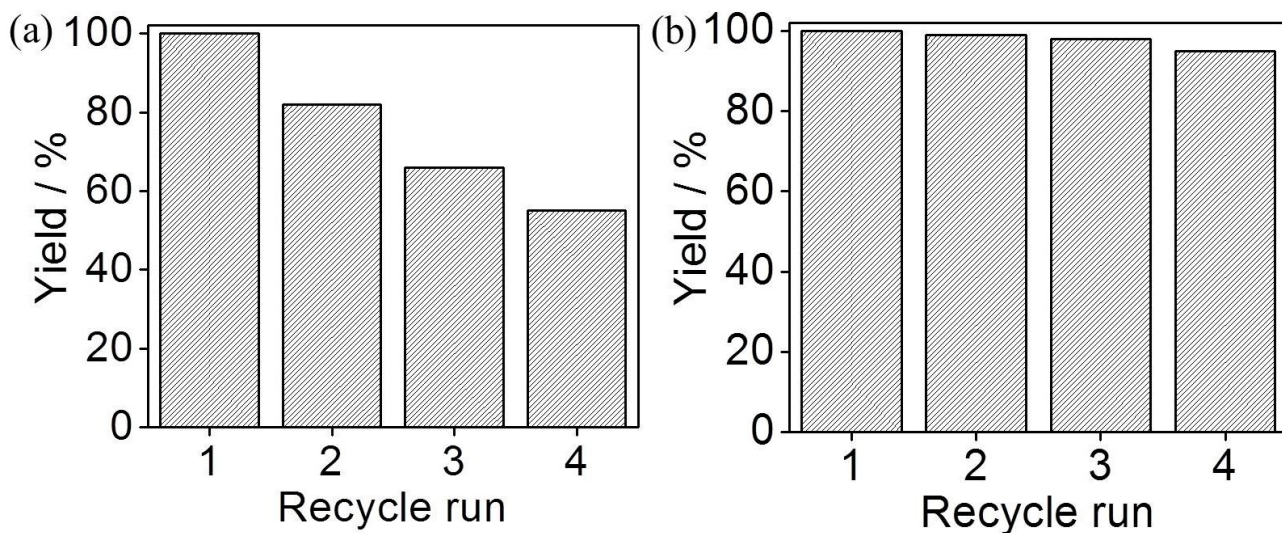


**Fig. S19.** (a) Reuse of  $\text{CoS}_2/\text{PC}$ , 8 h for each cycle, and (b) 16 h for each recycle. Reaction conditions: 2 mmol substrate, 3.7 mol % Co, 5 mL  $\text{CH}_3\text{OH}$ , 110 °C, 3 MPa  $\text{H}_2$ .

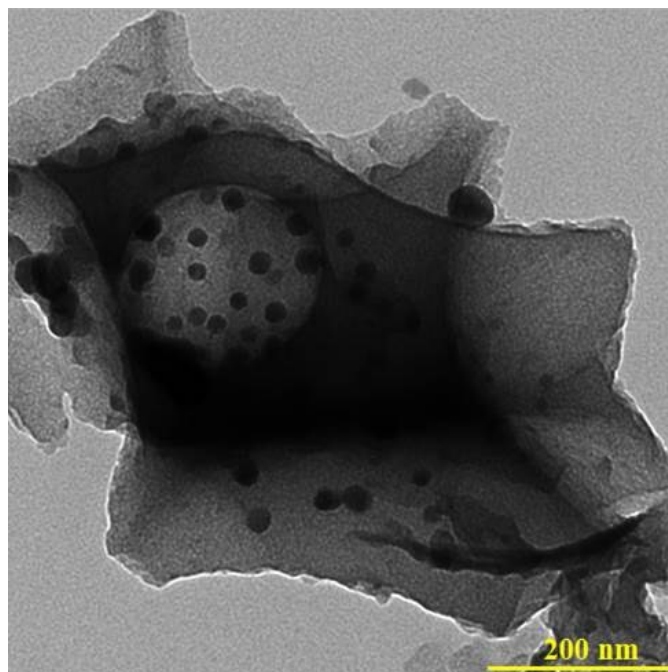


**Fig. S20.** TEM image of the recycle catalyst,  $\text{CoS}_2/\text{PC}$ .

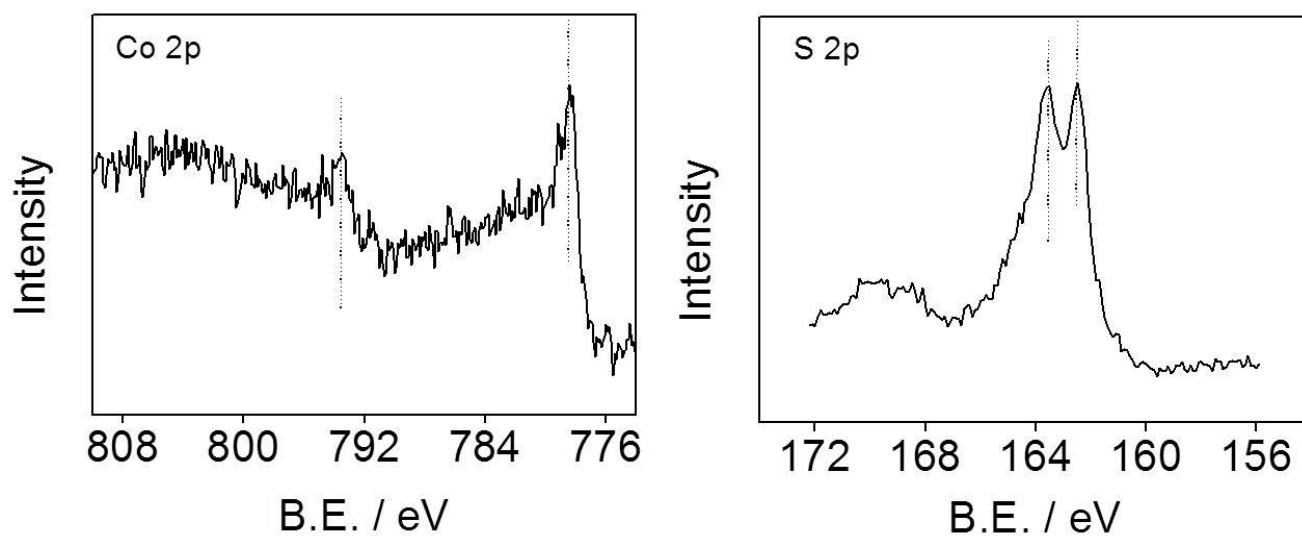
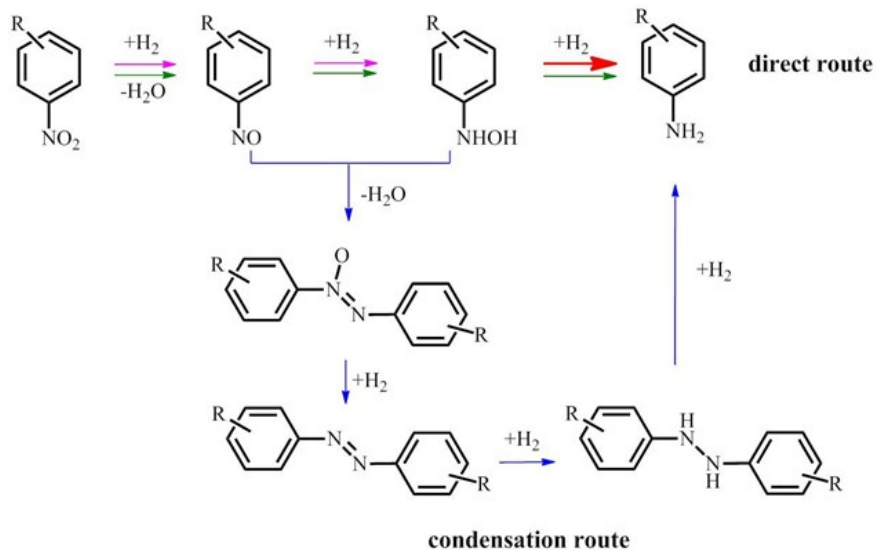


**Fig. S21.** XPS spectra of the recycle catalyst,  $\text{CoS}_2/\text{PC}$ : a) Co 2p spectrum; b) is S 2p spectrum.



**Scheme S1.** Reaction pathways proposed by Haber for the reduction of nitroarenes to the corresponding anilines.

**Table S1.** The Co, Fe and Ni content in different catalysts.

catalyst	ICP-AES results
CoS <sub>2</sub> /PC	14.8%
FeS <sub>2</sub> /PC	14.0%
NiS <sub>2</sub> /PC	12.5%

**Table S2.** Optimization parameters for the hydrogenation of 3-nitrostyrene catalyzed by CoS<sub>2</sub>/PC<sup>a</sup>.

Entry	Solvent	T (°C)	P (MPa)	Conv. (%) <sup>b</sup>	Sel. (%) <sup>b</sup>
1	Methanol	110	3	>99	>99
2	Methanol	100	3	54	>99
3	Methanol	90	3	36	>99
4	Methanol	110	1	33	>99
5	Methanol	110	2	45	>99
6	H <sub>2</sub> O	110	3	>99	>99
7	Dioxane	110	3	15	>99
8	Ethyl Acetate	110	3	63	>99
9	Toluene	110	3	22	>99
10	n-Hexane	110	3	18	>99

<sup>a</sup>Reaction condition: 0.5 mmol 3-nitrostyrene, 3.7 mol% Co, 3 mL solvent. <sup>b</sup> Determined by GC (internal standard: n-dodecane).

**Table S3.** Competitive hydrogenation of nitrobenzene and styrene using CoS<sub>2</sub>/PC <sup>a</sup>

feeding (mmol)		conversion (%) <sup>b</sup>	
styrene	nitrobenzene	styrene	nitrobenzene
0	0.5	-	100
0.5	0.5	1	100
0.5	0	4	-

<sup>a</sup> Reaction conditions: 3.7 mol% Co, 3 mL CH<sub>3</sub>OH, 110 °C, 3.0 MPa H<sub>2</sub>, 4 h. <sup>b</sup> Determined by GC (internal standard: n-dodecane).

**Table S4.** Practical Co and S content in the catalysts.

element	fresh (wt %)	recycle (wt %) <sup>a</sup>
Co	14.8	12.4
S	14.6	11.2

<sup>a</sup>The Co and S content in CoS<sub>2</sub>/PC after recycles.

---